

# LP TURBINE LAMINAR SEPARATION BUBBLE STUDY: FLAT PLATE DNS CALCULATIONS AND PRELIMINARY PIV DATA

*Tobias Ries<sup>1</sup>, Jenny Baumann<sup>1</sup>, Martin Rose<sup>1</sup>,  
Ulrich Rist<sup>2</sup>, Stephan Staudacher<sup>1</sup>*

<sup>1</sup>Institut für Luftfahrtantriebe, Universität Stuttgart  
Pfaffenwaldring 6, 70569 Stuttgart, Germany

<sup>2</sup>Institut für Aerodynamik und Gasdynamik, Universität Stuttgart  
Pfaffenwaldring 9, 70569 Stuttgart, Germany

## ABSTRACT

Laminar separation bubbles form on the back surfaces of aero-engine LP turbine blades. In recent years increasing lift coefficients have given significant weight and cost reductions and performance improvements have been achieved through a better understanding of the behaviour of such separation bubbles. A project is underway at Stuttgart University to study a possible technique to suppress the laminar separation bubbles using actuated transition. As a first step this paper reports on numerical and preliminary experimental results with and without actuation. DNS predictions are presented which show a significant influence on the separation size, revealing details of the transitional process. Also preliminary PIV data of a flat plate simulation of a turbine blade suction surface with laminar separation is presented.

## NOMENCLATURE

$A(h, k) = \bar{A}(h, k) / \bar{U}_\infty$	[-]	Amplitude of the spectral mode $(h, k)$
$c_D$	[-]	Diffusion coefficient
$\bar{f} = f \cdot \bar{U}_\infty / (\bar{L}_{DNS} \cdot 2 \cdot \pi)$	[Hz]	Disturbance frequency
$h$	[-]	Index for spectral mode in time
$k$	[-]	Index for spectral mode in $\bar{z}$ -direction
$\bar{L}_{gl}, \bar{L}_{DNS}$	[m]	Reference length global / for DNS
$M$	[-]	Mach number
$\bar{p}_0, \bar{p}_{throat}$	[N/m <sup>2</sup> ]	Static pressure after diffusion / Static pressure throat
$Re$	[-]	Reynolds number
$\bar{s}_c$	[m]	Chord length
$\bar{t}$	[s]	Time
$Tu$	[-]	Turbulence level
$\bar{U}_\infty$	[m/s]	Free stream velocity, reference velocity DNS
$\bar{U}_{gl}$	[m/s]	Global reference velocity
$\bar{u}, \bar{v}, \bar{w}$	[m/s]	Velocity in $\bar{x}, \bar{y}, \bar{z}$ direction
$\bar{x}, \bar{y}, \bar{z}$	[m]	Streamwise, wall-normal, spanwise coordinate
$-$		Dimensional value
$\alpha_i$	[-]	Amplification factor
$\alpha$	[-]	Dimensionless streamwise wave number
$\gamma$	[-]	Dimensionless spanwise wave number
$\bar{\nu}$	[m <sup>2</sup> /s]	Kinematic viscosity
$\bar{\omega}$	[1/s]	Vorticity
$\bar{\rho}$	[kg/m <sup>3</sup> ]	Density
$DNS$		Direct Numerical Simulation
$(h, k)$		Fourier modes in frequency-spanwise-wavenumber spectrum

## INTRODUCTION

Laminar separation bubbles on the suction sides of aero-engine LP turbine blades became more significant in the recent past due to low Reynolds numbers in small, high flying business jets and micro gas turbines as used in Unmanned Aerial Vehicles. Low Reynolds numbers of about 50,000 in such turbines in combination with reducing blade numbers and higher turning cause the laminar boundary layer in LP-turbines to separate. Many detailed investigations on steady and unsteady blowing in a cascade have been published, (Rist, Augustin, 2005), (Rivir, Sondergaard, 2004), (Rizetta, Visbal, 2005), (Volino, 2003), (Zhang, Vera, Hodson, 2005), (Vera, Zhang, Hodson, 2005). In several experiments synthetic jets are used to form streamwise vortices which transport fluid of high kinetic energy into the separation bubble to minimize or even eliminate it. In contrast to that we consider small disturbances of ideally zero net-mass flow with distinct frequencies which accelerate the laminar turbulent transition process so that the earlier turbulent boundary layer leads to a reduced separation. In the current study the combination of PIV and hot wires as well as hot film measurements in a low-speed wind tunnel along with DNS-Calculations of this flow will give a fundamental understanding of the processes leading to laminar-turbulent transition in a disturbed LP-turbine. The conditions of the LP-turbine are simulated by a profile on the opposite wall of the the flat plate on the bottom of the wind tunnel. Such a setup using a profile on the opposite wall has been used successfully before by (Lang, 2005). In this study the profile produces a pressure distribution similar to the distribution in an LP-Turbine. A separation bubble forms on the flat plate which is to be influenced by disturbances, small in amplitude and of a certain frequency brought in shortly before the separation bubble. On one hand the diffusion at the end of the LP-turbine causes the laminar boundary layer to separate, on the other hand small disturbances are amplified, leading finally to transition and a more stable boundary layer. Such small disturbances are present in every real flow, but exciting the right frequency at the beginning of the diffusion can lead to an earlier laminar-turbulent transition and therefore a smaller separation bubble without the need of a high air mass-flow, in contrast to steady blowing. The environment in a real turbine is still very different with respect to the rig. There are high levels of free-stream turbulence, periodic disturbances (potential and vortical) and noise as well as surface roughness. These issues must be resolved before engine application is seriously studied. In this paper the numerical and experimental design and setup is shown and first results are presented. For the experiment, the physical setup, the measurement technique and preliminary PIV measurements are provided. The experiment is due to unfortunate circumstances still in an early stage. Therefore just preliminary results of this work in progress are presented, until now without quantitative connections to the DNS-calculations. From the numerical side the design of the opposite profile is explained, the numerical setup for RANS and DNS calculations is shown and undisturbed, as well as disturbed DNS-calculations are presented.

## BASIC SETUP

### Design of the opposite profile

One of the first steps in the project was the development of the profile on the opposite wall of the flat plate (figure 1). It first causes an acceleration by narrowing the channel in  $\bar{y}$ -direction and then a diffusion by widening again. At two positions in  $\bar{x}$ -direction bleeds were built in. At the beginning of the flat plate a boundary layer bleed is necessary to get a new boundary layer as at the leading edge of a turbine blade. The second bleed is placed on the opposite profile in the diffusion zone to insure that the laminar separation bubble forms on the flat plate and not on the top profile. The aim was to reproduce the  $c_p$ -distribution of a typical LP-turbine blade (T161). Though the original  $c_p$ -distribution cannot be exactly reproduced due to the potential effect of the streamline curvature around the profile to the flat plate, the inflection points, the total acceleration and the diffusion coefficient  $c_D$  (equation 1) of 0,35 were reproduced as close as possible (figure 2).

$$c_D = \frac{P_0 - P_{throat}}{\frac{1}{2} \rho v_{throat}^2} \quad (1)$$

The profile was designed in an iterative process. The starting point was a flat plate with a boundary layer bleed on the lower wall and a cubic spline on the upper wall defined using twelve nodes. The nodes are not equally spaced, but accumulated at the narrowest section. Starting with a rough spline estimation of the required velocity values after Bernoulli's Theory, a coarse 2D-flow field was solved with a steady RANS-Solver (CFX). The  $c_p$ -distribution at the wall then was compared with the  $c_p$ -distribution of the LP-turbine blade, the nodes were adjusted and the new profile was calculated again. This first quick iterative process was repeated till the  $c_p$ -distributions were as close as it could be expected with the coarse grid of 223 nodes in  $\bar{x}$ -direction and 50 nodes

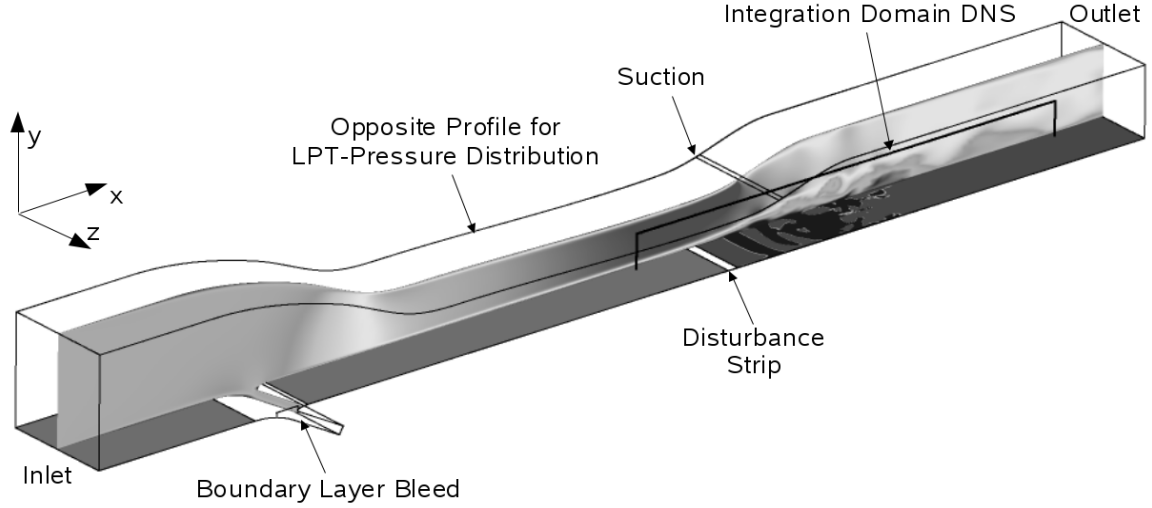


**Figure 1: Model of wind tunnel with DNS-integration domain and disturbance strip**

in  $\bar{y}$ -direction. Then iterations were continued with a refined and redistributed 2D-grid using 287 nodes in  $\bar{x}$ - and 62 nodes in  $\bar{y}$ -direction. 3D calculations are necessary to check that the flow is two-dimensional in the middle of the wind tunnel. For these simulations first a grid with 410 nodes in  $\bar{x}$ -, 62 nodes in  $\bar{y}$ - and 150 nodes in  $\bar{z}$ -direction representing the original geometry of the channel was used. This was finally refined and redistributed to 1104 nodes in  $\bar{x}$ -, 45 nodes in  $\bar{y}$ - and 113 nodes in  $\bar{z}$ -direction. As turbulence models  $k-\omega$  based SST (shear stress transport) and a simple mixing length model were applied. As expected the flow field is very dependent on the free stream turbulence and the turbulence model. So there was an uncertainty on how the channel would respond in reality. But on the other side it also turned out that the bleed-mass-flow on the profile provides the opportunity to control these uncertainties in a wide range. By the variation of its mass flow the size of the separation bubble can be varied significantly. The boundary layer bleed upstream was adjusted to keep the stagnation point correctly positioned on the leading edge of the flat plate. The leading edge shape was changed from circular to elliptic, to reduce the probability of a leading edge separation. Another possibility to avoid separation on the upper profile would have been to use turbulators. But with this solution control of the size of the undisturbed separation bubble wouldn't have been possible and also unwanted disturbances might have propagated into the laminar boundary layer on the flat plate, influencing the transition process. The inlet to the wind tunnel is held fixed as  $0.1\text{m}^2$ . Therefore the required variation of the channel height to match the  $c_p$ -distribution was done at the exit. That way the exit velocity and with it the Reynolds number changed continuously during the layout process, which is the reason why the layout-Reynolds-number (equation 2) was defined over the inlet velocity which is unusual for turbines. The design inlet velocity was set to  $\bar{U}_{inlet}=1.0\text{m/s}$ , the reference length to  $\bar{L}_{design}=0.54\text{m}$  and the reference kinematic viscosity to  $\bar{\nu}=1.5\cdot 10^{-5}\text{m}^2/\text{s}$  which results in a reference Reynolds number of 36,000. Taking the velocity at exit, it would be 79,164, but this is easily adjustable in the wind tunnel by changing the velocity.

$$Re = \frac{\bar{U}_{gl} \cdot \bar{L}_{gl}}{\bar{\nu}} \quad (2)$$

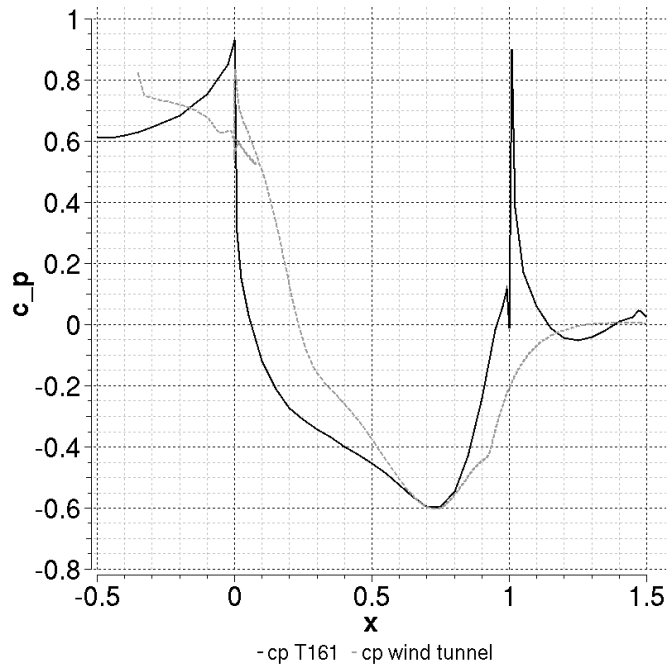


**Figure 2:  $c_p$ -distribution comparison T161 - wind tunnel with profile.**

## DNS – NUMERICAL INVESTIGATIONS

### Intention

The purpose of the DNS-Simulations is to gain a detailed insight into the laminar-turbulent transition mechanisms at a fundamental level that take place when actuation is applied to separation bubbles at a LP-turbine like  $c_p$ -distribution. The simulation analysis provides the exact development of the amplified disturbances within the flow and interactions between different disturbances. From this data the transition process can be analyzed for the different actuation settings to find out how the transition process and its length is affected by the parameter variations. In addition the flow field can be visualized unsteadily and by averaging over one period the average separation bubble size can be determined.

### Code

The code used for the DNS-calculations is *n3d* provided by the IAG (Institut für Aerodynamik und Gasdynamik, Universität Stuttgart). It is the institutes standard tool for accurate simulation of laminar turbulent transition and has proved to be reliable in various applications. It is an unsteady, incompressible 3D-Navier-Stokes-Solver with 4<sup>th</sup> order discretization in time, 6<sup>th</sup> order in  $x$ - and  $y$ -direction and a spectral resolution in  $z$ . Detailed information is available in (Augustin, 2005), (Kloker, Konzelmann, Fasel 1993), (Kloker, 1998), (Rist, Maucher, Wagner, 1996), (Rist, Maucher, 2002).

### Discretization

For the numerical discretization in  $x$  and  $y$ -direction a finite-difference discretization in physical space is used, but the spanwise discretization takes place in Fourier-space. So the spanwise ( $z$ ) direction is solved for a certain frequency. Resolution in  $z$ -direction is increased by solving for multiple frequencies, such that the resolved resolution is determined by the spanwise wavelengths and the Nyquist criterion. The integration domain is also symmetric by definition due to the use of Fourier coefficients. The standard grid for the long integration domain contains 706 nodes in  $x$ -direction and 289 nodes in  $y$ -direction. In the spanwise direction in this paper two modes were

solved for being able to capture the influence of a three-dimensional mode in the breakdown scenario. To make sure that more modes in spanwise direction are not absolutely necessary for the calculations presented in this paper, the reference case was calculated with eight modes as well. It turned out that the differences didn't affect the conclusions.

### Integration Domain

The integration domain for the DNS-calculations is a rectangular block consisting of an equidistant grid in  $x$ - and  $y$ -direction as can be seen in figure 3. It starts  $360\text{mm}$  behind the flat plate leading edge and is  $237\text{mm}$  long. The height is  $30\text{mm}$ . To obtain results which are independent of the integration area, the height of the separation bubble needs to be significantly smaller than the integration domain. So the top of the integration domain was set to the maximum extent of the channel where the upper boundary layer is just not influencing the prescribed velocity boundary layer. All values in the diagrams are made non-dimensional with  $\bar{L}_{DNS}=0.061\text{m}$ ,  $\bar{U}_\infty=2.59038\text{ m/s}$  and  $\bar{\nu}=1.5\cdot 10^{-5}\text{ m}^2/\text{s}$ . Due to program internal reasons the  $x$ -coordinate is also shifted by  $\Delta x=-3.56$ .

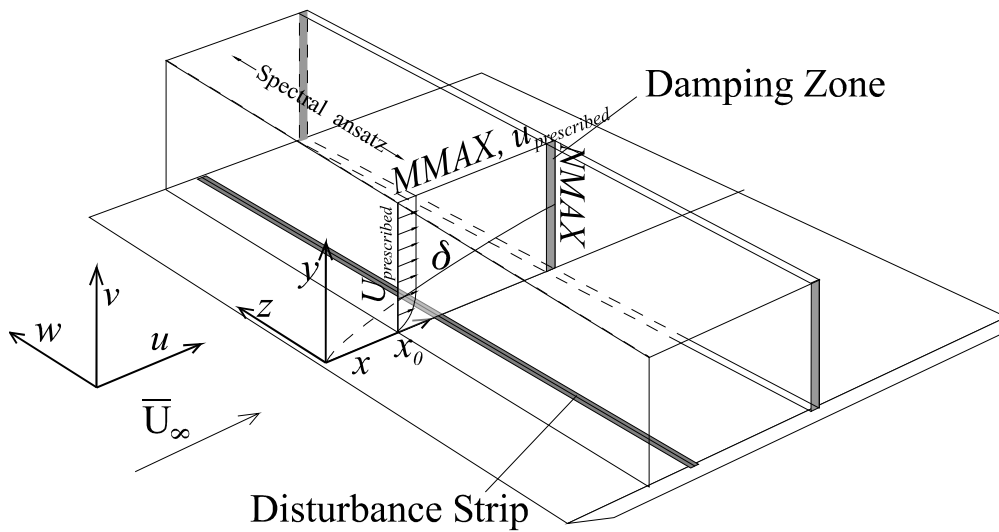


Figure 3: DNS integration area scheme

### Boundary Conditions

The rectangular grid requires input for the boundary conditions at the left hand and the top edge. At the left hand edge, a boundary layer velocity profile is prescribed by  $u$ ,  $v$  and  $\omega_z$ . It is an accelerated laminar boundary layer velocity profile taken from the RANS-Simulations mentioned above, but will be replaced by the experimental boundary layer when the data is available. At the top, a  $u$ -velocity distribution is prescribed (figure 3). There is an acceleration area at the beginning and an area of strong deceleration at the end as can be seen in the  $c_p$ -distribution in figure 2. The lower edge is determined by the no-slip condition, except at the disturbance strip where disturbances are brought into the fluid by exciting  $v$  at the wall in time with the disturbance frequency. In  $x$ -direction these disturbances are of a half or complete sinusoidal shape and in spanwise direction with periodic waves with a multiple of the base spanwise wavenumber. At the right hand edge the pressure is set in such a way that conservation of mass is fulfilled and a damping zone is used to eliminate possible reflections of disturbances (M. Kloker, Konzelmann, Fasel, 1999).

### DNS – Frequency Analysis

Decelerated flows react sensitively on disturbances of certain frequencies. Once excited, they get amplified exponentially by linear growth mechanisms (Rist, 1998). Linear means that the disturbance amplitude is proportional to the initial amplitude at any position. So, no nonlinear interactions between different frequencies are taking place at this stage. Due to this linear nature, the frequencies which are sensitive to such amplification can be obtained by a stability analysis of

the flow field. This means replacing the velocities in the Navier-Stokes-equations by a mean flow and a disturbed flow, taking just the linear parts of the resulting equation, adopting a harmonic solution and solving iteratively for the eigenvalues of the resulting equation. This provides the amplification factor  $\alpha_i$  for a given frequency at a given point in streamwise direction of a flow field. With this information the optimal point and the according frequency of maximal amplification

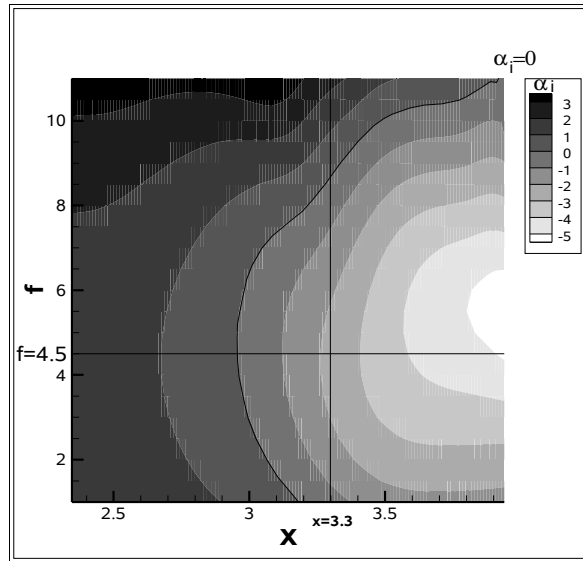


**Figure 4: Stability diagram**

can be obtained. The stability solver for this investigation was *icostab* provided by the IAG. As base-flow for the frequency analysis a converged stationary 2D-simulation with the boundary conditions mentioned above was taken. To obtain a converged, stationary solution a shorter integration domain had to be used. It was cut off at  $\bar{x}=456mm$  after the leading edge which is the point where strong deceleration starts, just before the beginning of the separation bubble. For the given flow field an optimal dimensionless frequency of  $f=4.5$  was found promising optimal amplification downstream from a position of  $x=3.3$  (figure 4). The transformation of this frequency to a real turbine environment results in very high frequencies ranging from about  $40kHz$  to  $85kHz$ , depending on the turbine environment. There is no known solution yet to realize such high frequencies in a turbine.

### DNS – Analysis

The fundamental question of this project is the influence of actuation on a laminar separation bubble on an LP-turbine blade. Comparisons between actuated and non-actuated separation bubbles can show the effects of actuation on the bubble. In addition, different types of actuation can lead to significant differences in the solutions. Therefore, a matrix of different actuation scenarios was set up to obtain more knowledge about the transition mechanisms. The actuation frequency and amplitude was varied, actuation was switched off, and the position of actuation was changed. In the following sections the first results of these calculations are presented. In the figures 5, 6 and 8 amplification curves are plotted. The abscissa represents the streamwise direction  $x$ , the ordinate the maximal amplitude in  $y$  of the Fourier analyzed frequency over one actuation period. An amplitude of  $1.0$  would imply a maximal disturbance velocity of the reference velocity  $\bar{U}_\infty$ . The notation is  $(h,k)$ , where  $h$  represents multiples of the fundamental 2D mode and  $k$  multiples of the spanwise fundamental mode. So  $(1,0)$  would be a 2D-fundamental mode,  $(1/2,1)$  the subharmonic 3D wave with half of the fundamental wavelength  $\alpha$  and the spanwise wavelength  $\gamma$ .

### Undisturbed flow

In figure 5 the fundamental excitation plot of an undisturbed calculation is plotted. Undisturbed means a very weak disturbance of  $A=1.0 \cdot 10^{-10}$  which was proven to have no influence on the result. Such an unsteady flow simulation with the boundary conditions described above leads to a big separation bubble which doesn't reattach within the integration area. The flow doesn't show periodic behavior even after long simulation times. The separation bubble gets very big and even reaches the upper limit of the integration zone, which influences the result. Due to this non-periodic behavior the plot is not completely independent in time. A critical amplitude of  $A=1.0 \cdot 10^{-1}$  is not reached before  $x=5.6$ .

### Variation of the actuation frequency

According to the frequency analysis exciting with a frequency of  $f=4.5$  should result in amplification and highest integral amplification of the disturbed fundamental mode. In figure 6 the amplification curves of the excitation fundamental (1,0) frequencies  $f=4.0$ ,  $f=4.5$  and  $f=5.0$  are plotted. After the relatively strong disturbance input of  $A=1.0 \cdot 10^{-2}$  at  $x=3.27$  (414mm from flat plate leading edge) there is a short plateau where the mode is not amplified. Then, from  $x=3.7$  on, the modes of  $f=4.5$  and  $f=5.0$  start to grow from almost exactly the same position on with an

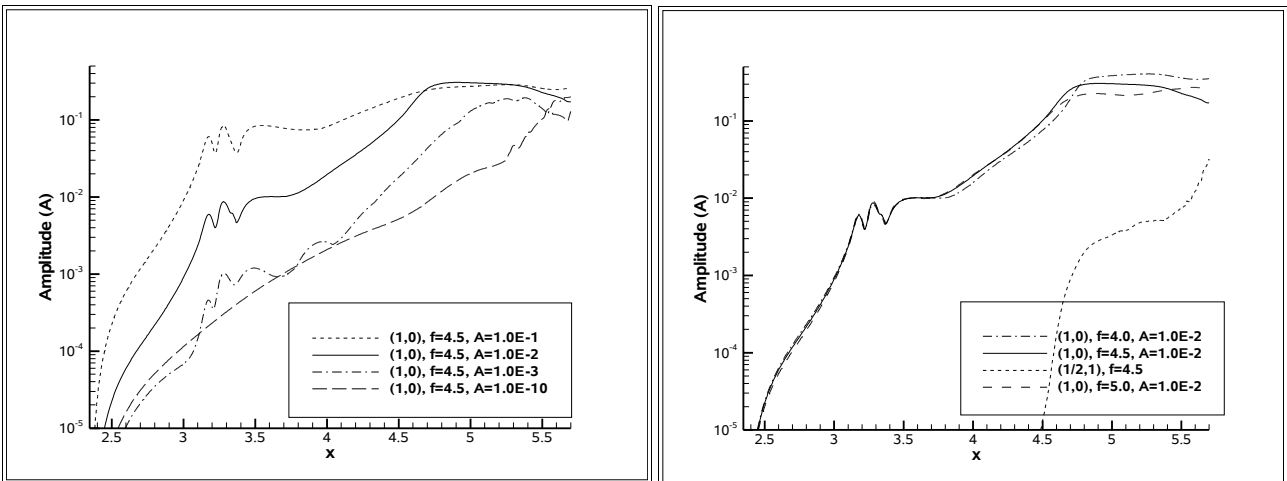


**Figure 5: Influence of disturbance amplitude on the fundamental modes**

**Figure 6: Influence of disturbance frequency on the fundamental modes**

identical growth rate. This is true up to the critical amplitude of  $A=1.0 \cdot 10^{-1}$  at  $x=4.5$  where the amplitude plot for  $f=4.5$  continues to grow with a slightly increased rate up to an amplitude of  $A=3.0 \cdot 10^{-1}$  at  $x=4.85$  whilst the plot for  $f=5.0$  reduces in growth rate and reaches its maximum at  $A=2.2 \cdot 10^{-1}$  at about the same position. This indicates, that due to the higher growth rate at the end  $f=4.5$  is slightly better for providing early transition compared to  $f=5.0$ . As an example for the typical behavior for the subharmonic 3D modes,  $A(1/2,1)$  for the case  $f=4.5$ ,  $A=1.0 \cdot 10^{-2}$  is plotted in figure 6. It doesn't reach high amplitudes in the whole flow field and therefore doesn't have a big influence. The fundamental of  $f=4.0$  starts to grow at  $x=3.81$ , so slightly later than the other two, but with the same growth rate. Like  $f=4.5$ , it starts to grow faster at  $x=4.55$  and even reaches a higher saturation amplitude of  $A=4.0 \cdot 10^{-1}$  than  $f=4.5$  but later at  $x=5.2$ . So the frequency of  $f=4.5$  seems to be the most suitable for reaching early transition with high amplification which fits to the findings of the stability diagram.

### Variation of the actuation amplitude

The investigation of the influence of the actuation strength on the transition is necessary because a too weak disturbance might not be capable to control the laminar turbulent transition position. On the other side a very strong disturbance would in reality be expensive in terms of actuation technology, realization, efficiency or energy required. In addition, it might simply cause bypass

transition whilst the aim of this project is to reach transition by instability modes with low energy input. Results of three calculations are plotted in figure 5. Compared to the reference case, the amplitude was lowered and increased by an order of magnitude. The amplitudes were  $A=1.0 \cdot 10^{-1}$ ,  $A=1.0 \cdot 10^{-2}$  (reference case) and  $A=1.0 \cdot 10^{-3}$ . Compared to the reference the excitation with  $A=1.0 \cdot 10^{-3}$  already shows the problem described above. The excitation of the disturbance is still clearly observable, but unlike in the cases with higher disturbance amplitudes, it is not able to force the flow into strong periodic behavior any more. Whilst the fundamental of the reference case is independent to the analyzed period in time, for the case with  $A=1.0 \cdot 10^{-3}$ , the general shape of the amplification plots stay the same, but there is a significant variation depending on the period. The flow still forms the downstream rolling waves of the disturbed frequency but is not strictly periodic any more. Disturbing earlier, as described in the next paragraph, also doesn't solve that problem.

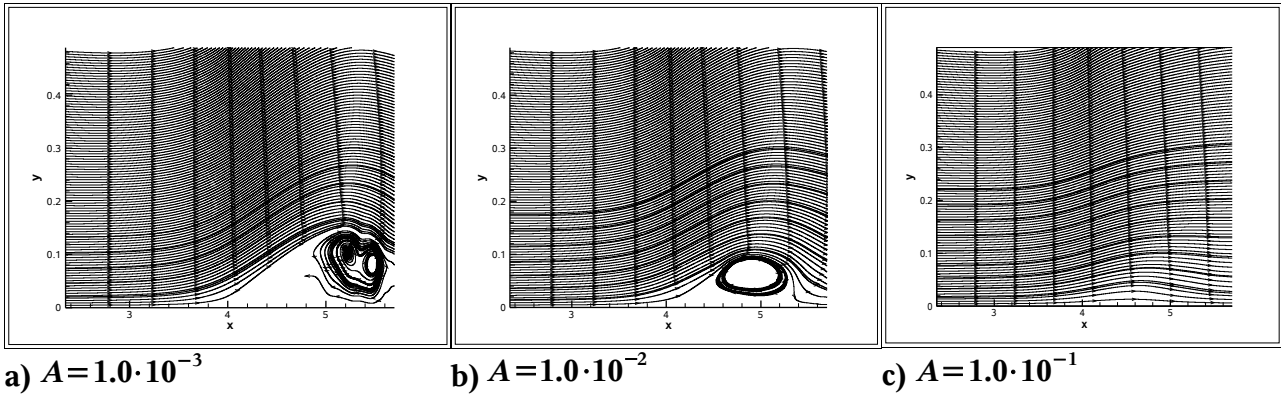


**Figure 7a,b,c: Time averaged streamlines**

A further reduction of the amplitude results in uncontrolled behavior. The excited frequency is not able to dominate the flow field any more, different disturbances get excited and lead to uncontrolled, later transition as in the undisturbed case described below. With a high disturbance amplitude of  $A=1.0 \cdot 10^{-1}$ , like in the case with  $A=1.0 \cdot 10^{-2}$  after the disturbance strip there is first a zone of moderate damping in the amplitude plot before the excitation starts at  $x=3.95$ , slightly later than for  $A=1.0 \cdot 10^{-2}$ . The amplification rate is much lower than in the reference case, so that the critical amplitude of  $A=1.0 \cdot 10^{-1}$  is already reached after a short distance. But this is simply the result of the high disturbance amplitude of  $A=1.0 \cdot 10^{-1}$ . Saturation is not reached earlier than with  $A=1.0 \cdot 10^{-2}$  due to the lower amplification rate. Nevertheless, the separation bubble gets continuously smaller with an increase in amplitude, as the comparison between the time averaged flow fields in the figures 7a),b),c) show for the different amplitudes. It can be concluded, that the disturbance amplitude has a lower limit at about  $A=1.0 \cdot 10^{-3}$  below which the early transition caused by the modal instability doesn't work any more. Over that limit, the disturbed frequency is coupled in properly and grows quickly up to saturation. There doesn't seem to be an apparent upper limit for the actuation, but the growth rate reduces at very high disturbance amplitudes and since minimizing the amount of energy required is desirable, the use of small disturbances would be more efficient.

Variation of the actuation position

The position of the disturbance input is another variable where change could lead to differences in the result. In figure 8 the amplification plot for the fundamental modes (1,0) of four cases are plotted. First, the reference case with  $A=1.0 \cdot 10^{-2}$  was taken and the position of the disturbance strip was shifted from  $x=3.27$  (414mm from flat plate leading edge) further upstream to  $x=2.68$  (378mm from leading edge). The early actuation reaches the same excitation amplitude as the late actuation, but instead of starting to grow, it remains almost on the same level with a small amplitude decay up to the position where the later disturbed case starts to grow. Then it grows with the same amplification as in the later disturbed case, from a slightly lower amplitude. This leads to

the fact, that saturation is reached slightly later at  $x=5.05$  compared to  $x=4.85$  in the reference case. Therefore it can be concluded that the actuation position doesn't have a strong influence on the transition mechanism in this case, but too early disturbance can delay transition. If the actuation would take place too far upstream there might be the risk that the damping caused by the free stream acceleration reduces the disturbance so much that it couldn't cause transition any more as explained above. This behavior was also observed with a disturbance amplitude of  $A=1.0 \cdot 10^{-3}$ , also plotted in figure 8. This case was calculated to find out whether an earlier disturbance, which would have more time to grow before separation, could lower the minimal required amplitude. But also at the lower amplitude, the mode doesn't begin to grow before  $x=3.7$ . In addition the flow doesn't converge to a strong periodic behavior as well as in the previous case with  $A=1.0 \cdot 10^{-3}$  at the later position. This confirms the existence of a minimal required disturbance amplitude of about 1% of the reference velocity.

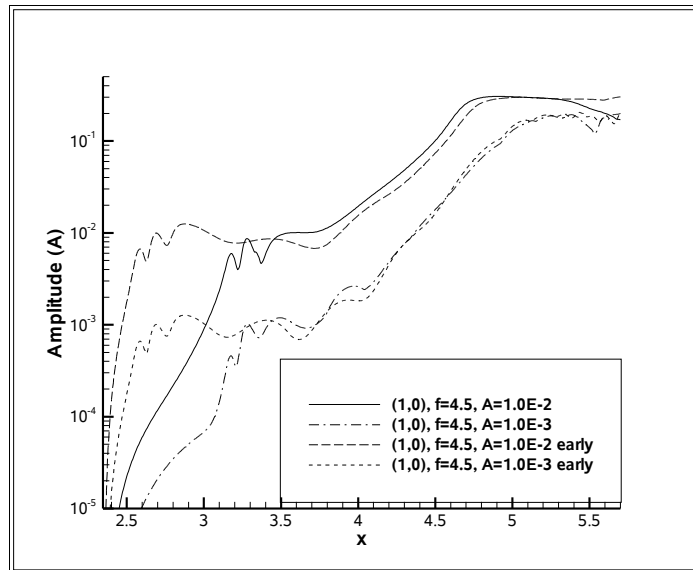


**Figure 8: Influence of disturbance position on the fundamental modes**

### Comparison actuated – non-actuated flow.

In figure 6 the fundamental excitation plot of an undisturbed calculation is plotted together with the reference case of  $f=4.5$ . The fundamental wave of the undisturbed case reaches high amplitudes much later than in the disturbed case. Whilst in the disturbed case an Amplitude of  $A=1.0 \cdot 10^{-1}$  is already reached at  $x=4.5$ , the corresponding mode in the undisturbed case doesn't reach it before  $x=5.6$ . Other frequencies might be more dominant in the undisturbed case, but no other modes were found to be higher at an earlier position. As mentioned above, the separation reached the upper limit of the integration zone. So the accuracy of the value of  $x=5.6$  is questionable, but not the fact that transition without disturbance takes place much later.

## **EXPERIMENTAL SETUP**

### **Test Section**

For the experimental setup an existing wind tunnel was modified. The cross section as well as the length of the test section therefore was fixed. A modular bottom plate was designed to ensure easy changeability of the modules containing actuation or instrumentation respectively. The layout process of the geometry of the profiled wall and both boundary layer suction has already been described above. Since an optical measurement technique is to be used, the profiled wall and one of the side walls are made of Perspex to enable optical access.

## Inlet Plenum

The wind tunnel is sucking air from the test hall. Given that changing environmental conditions (which can not be held constant) were heavily influencing the behaviour of the sucked air, an inlet plenum was designed to cut off these influences. Its cross section is ten times as big as those of the test section. A cut through the plenum and test section as well as the arrangement of the built-in components are shown in figure 9. Unlike in most laminar flow test rigs the inlet of the plenum (1) is smaller (1/100) than the cross section of the tunnel. Forcing the air through it and therewith highly increasing the speed of the sucked air is to eliminate environmental disturbances from the flow. Using perforated plates as baffles (2) the fluid is forced to spread over the whole cross section of the plenum. With round shaped (3mm diameter, 50mm length) honeycombs (3) and fabric screens (4) the now low speed flow is made uniform and the strong turbulences produced by the unusual inlet design are damped out, resulting in a turbulence level in the inlet of the test section of  $Tu \leq 0.1\%$ . The contraction from the plenum to the test section cross section is done by a sine-cosine passage. It enables a smooth acceleration of the flow and is unlikely to cause separation.

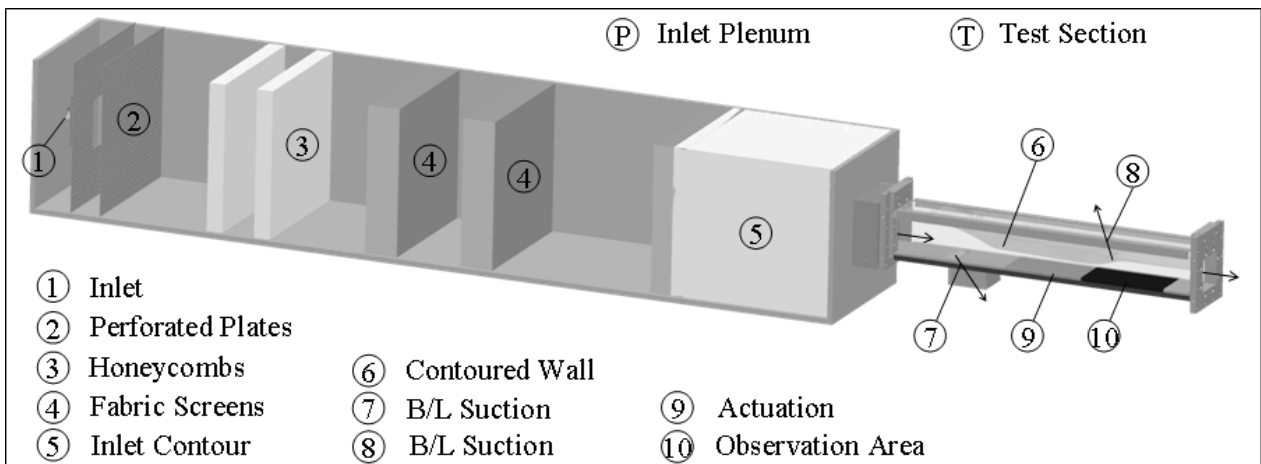


Figure 9: Schematic of the test rig

## Mass Flow Control

The controlling parameter for the experiments is the Reynolds number  $Re$  calculated from the main flow velocity  $\bar{v}$  and the chord length  $\bar{s}_c$  (i.e. profile length) from equation (2). The velocity in the test section depends on the mass flow which is set up by using orifice plates in the pipework downstream of the test section. Those orifice plates were designed for a defined total pressure in the test section under the assumption that the flow through them is critical ( $M=1.0$ ). Since the mass flow through the orifice plates depends on the total pressure in the test rig, the pressure has to be held constant to assure similar conditions for different test days. As already mentioned above, the environmental conditions in the test facility can't be held constant but are changing even in a day's time. A cone to enable the size of the inlet to be varied was designed as a solution for this problem. Changing the inlet area and holding constant the mass flow means changing the velocity of the fluid through the inlet. Since the pressure drop scales with the square of the velocity, a defined pressure in the test section can be set up by adjusting the cone depending on the ambient pressure.

## Actuation

The actuation is done with a loudspeaker setup where the oscillation of the loudspeakers membrane causes the air in a plenum on top of it to oscillate as well. Controlling this oscillation by the aid of a frequency generator, defined actuation frequencies can be produced. Observation of the general functionality was done with a microphone and an oscilloscope as diagrammed on the left hand side in figure 10. For future experiments, where the actuation is implemented in the test section, frequency generator and oscilloscope are replaced by a computer system, using the sound card. Investigation of frequency and amplitude will be done by the aid of hot wire measurements.

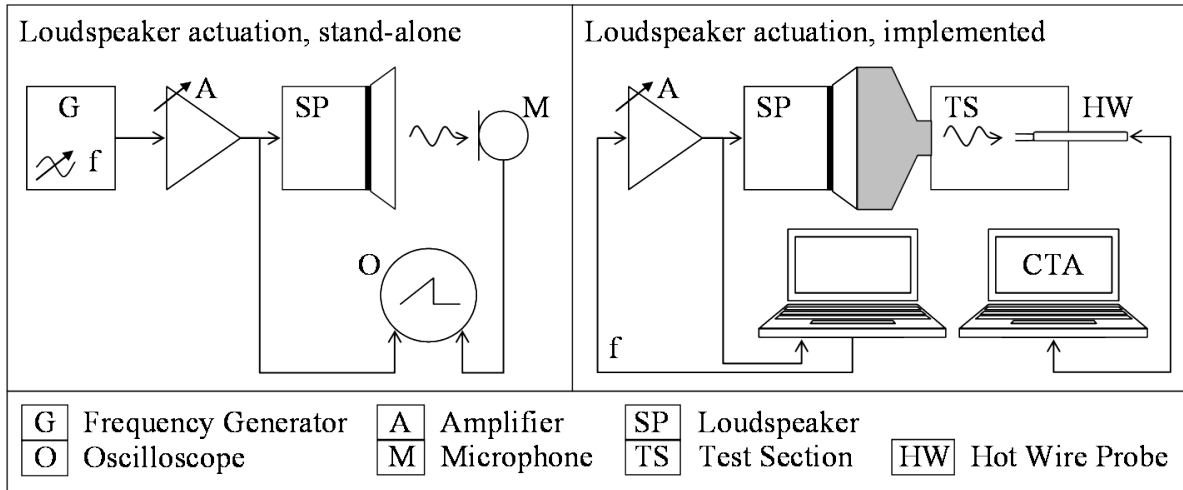


**Figure 10: Schematic of the loudspeaker actuation**

### Instrumentation

The main measurement techniques used to study the flow are hot wire/hot film measurements and Particle Image Velocimetry (PIV). PIV measurements are used to get the velocity vectors in a 2D flow field. The PIV software also enables the calculation of streamline pictures. Since the hot wire probe needs physical access to the test section, a second profiled wall with several closable holes has been made to replace the perspex profile. Traversing the hot wire probe in  $\bar{y}$ -direction, the boundary layer can be measured. The data is also used to calculate the turbulence level in the test rig. The turbulence level  $Tu$  of the flow field should not exceed 1% to have a laminar flow field. It is calculated from the standard deviations of the measured velocity components  $\bar{u}$ ,  $\bar{v}$  and  $\bar{w}$  and the mean free stream velocity  $\bar{U}_\infty$ .

$$Tu = \frac{1}{\bar{U}_\infty} \cdot \sqrt{\frac{1}{3} \cdot (\overline{u'^2} + \overline{v'^2} + \overline{w'^2})} \quad (3)$$

whereas

$$\overline{u'^2} = \frac{1}{n-1} \cdot \sum_{i=1}^n (\bar{u} - \bar{u}_i)^2 \quad (4)$$

For comparability with simulation also pressure measurements will be made. Static pressure is measured in four relevant positions in streamwise direction (plenum, test section inlet, throat and defined “end of blade”) while the total pressure is only measured in one position. The Pitot probe for total pressure measurement is to sit in the plenum in front of the contraction and is used to control the pressure adjustment by the inlet area variation. Positions of the probes and tappings are marked in figure 11.

In addition to instrumentation, the setup of the loudspeaker actuation as well as their implementation into the test rig can be seen. The oscillation caused by the loudspeaker is brought into the test channel through a slot 350mm downstream the leading edge, near the throat of the test channel flow. The current slot is shaped rectangular (width = channel width, length = 0.3mm) while the outflow angle is orthogonal to the flow direction. Other geometries and angles are to be investigated as well.



figure 13 some example PIV measurement results are shown. An undisturbed flow field in the test rig without upper boundary layer suction is displayed in figure 13a). The separation bubble develops in the deceleration area on the upper wall. Sucking off the boundary layer causes the flow to adapt on this wall. As the separation causing pressure gradient is still present, the flow now separates on the opposite (bottom) wall as can be seen in figure 13b). An example picture of the effect of actuation (0.3mm slot, 350mm from leading edge, actuation frequency 30Hz) on this separation is shown in figure 13c). The streamlines near the bottom wall seem to go downwards. This effect cannot be seen in the vector pictures and therefore is a post-processing issue which will be solved in the future.

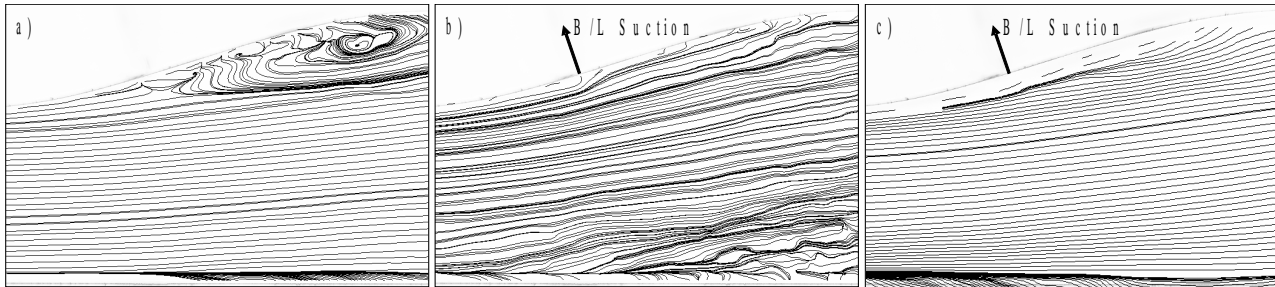


**Figure 13: Streamline pictures of the flow field a) without upper boundary layer suction, b) with boundary layer suction and c) with boundary layer suction and actuation**

## CONCLUSIONS

This paper contains numerical and experimental results. In the numerical part a low-Reynolds-number flow field in a rectangular wind tunnel with a  $c_p$ -distribution similar to a LP-turbine has been laid-out. Numerical simulations have been performed with a RANS-solver to obtain a flow field in the channel which provides the boundary conditions for the DNS-calculations before experimental data is available. With these boundary conditions, DNS calculations have been made, covering the area from shortly before the main flow deceleration to after the point of transition. The calculations have been made with and without disturbances. Disturbance frequency, amplitude and position have been changed to evaluate the effect on transition. To gather the right range of frequencies which would lead to best amplification and transition, a linear stability solver was used. It was found, that the predictions of the stability solver fit with the observations in DNS and that there is an optimal disturbance frequency. At a lower frequency fundamental growth starts later and at a higher frequency the maximal amplitude and growth rate shortly before saturation is lower. It was further found that the point of disturbance input is less important for the transition mechanism, but can delay transition. There is also a critical limit for the excitation amplitude. When it gets too small, the instability mode mechanism doesn't work any more. As next steps, the findings have to be reproduced and verified with experimental boundary conditions, further investigation is necessary on using a higher spanwise resolution and the influence of 3D-disturbances.

In the experimental part, a test rig to study turbine laminar separation with actuation has been commissioned. The inlet boundary condition is uniform and has low turbulence intensity ( $\leq 0.1\%$ ). Early results show the sensitivity of the laminar bubble to actuation. Although, as described in the introduction, the turbine environment is very different from the rig, it is concluded that the approach of actuated transition for laminar separation control in LP turbines shows some promise.

## ACKNOWLEDGEMENTS

The financial support of VITAL SP6, work package 6.4, task 6.4.3, the support of MTU Aero Engines and the possibility to use the stability solver icostab from Marcus Zengl, IAG is acknowledged.

## REFERENCES

1. K. Augustin, (2005), Zur aktiven Beeinflussung von laminaren Ablöseblasen mittels Grenzschichtstörungen, Dissertation, Institut für Aerodynamik und Gasdynamik, Universität Stuttgart.
2. M. Kloker, U.Konzelmann, H.Fasel, (1993), Outflow boundary conditions for spatial Navier-Stokes numerical simulations of transition boundary layers. *AIAA Journal* 31 (4), 620-628.
3. M. Kloker, (1998) A robust high-resolution split-type compact FD scheme for spatial direct numerical simulations of boundary layer transition, *Applied Scientific Research* 59 (4), 353-377.
4. Lang, M. (2005), Experimentelle Untersuchungen zur Transition in einer laminaren Ablöseblase mit Hilfe der Laser-Doppler-Anemometrie und der Particle Image Velocimetry. Dissertation, Universität Stuttgart, Verlag Dr. Hut, München.
5. U.Rist, (1998), Zur Instabilität und Transition in laminaren Ablöseblasen, Habilitationsschrift, Institut für Aerodynamik und Gasdynamik, Universität Stuttgart, Shaker Verlag.
6. U.Rist, K. Augustin, (2005), Control of laminar separation bubbles using instability waves, *Proc. ISABE-2005-1041*, *AIAA Journal* 44 (10), October 2006, 2217-2223
7. U.Rist, H.Fasel, (1995), Direct numerical simulation of controlled transition in a flat-plate boundary layer. *J. Fluid Mech.* 298, 211-248.
8. U.Rist, U.Maucher, S.Wagner, (1996), Direct numerical simulation of some fundamental problems related to transition in laminar separation bubbles. In *Computational Methods in Applied Sciences '96*, ECCOMAS Paris, France, John Wiley & Sons Ltd., 319-325.
9. U.Rist, U.Maucher, (2002), Investigations of time-growing instabilities in laminar separation bubbles. *European Journal of Mechanics B/Fluids* 21, 495-509.
10. R.B. Rivir, R. Sondergaard, (2004), Control of separation in turbine boundary layers, 2<sup>nd</sup> AIAA Flow Control Conference 2004, Portland, AIAA 2004-2201.
11. D.P. Rizetta, M.R.Visbal, (2005), Numerical simulation on separation control for transitional highly loaded low-pressure turbines, *AIAA Journal*, Vol. 43, 1958-1967.
12. M. Vera, X.F. Zhang, H. Hodson, (2005), Separation and Transition Control on an Aft-loaded Ultra-High-Lift LP Turbine Blade at low Reynolds Numbers: High-Speed Validation, *ASME Turbo Expo 2005*, Reno-Tahoe, GT2005-68893
13. R. Volino, (2003), Serparation Control on low-pressure turbine airfoils using synthetic vortex generator jets, *ASME Turbo Expo 2003*,Atlanta, GT2003-38729.
14. X.F. Zhang, M. Vera, H. Hodson, (2005), Separation and Transition Control on an Aft-loaded Ultra-High-Lift LP Turbine Blade at low Reynolds Numbers: Low-Speed Investigation, *ASME Turbo Expo 2005*, Reno-Tahoe, GT2005-68892